Imaging Native Calcium Currents in Brain Slices

Karima Ait Ouares, Nadia Jaafari, Nicola Kuczewski, Marco Canepari

HAL Id: hal-02441768
https://hal.science/hal-02441768

Submitted on 16 Jan 2020

2

3

4   ## *Imaging Native Calcium Currents in Brain Slices*

5

6   **Karima Ait Ouares**[a,b], **Nadia Jaafari**[a,b] , **Nicola Kuczewski**[c] and **Marco Canepari**[a,b,d]

7

8   [a] Univ. Grenoble Alpes, CNRS, LIPhy, F-38000 Grenoble, France

9   [b] Laboratories of Excellence, Ion Channel Science and Therapeutics, France.

10   [c] Centre de Recherche en Neurosciences de Lyon, INSERM U1028/CNRS UMR5292, Université

11   Lyon1, Lyon, France

12   [d] Institut National de la Santé et Recherche Médicale (INSERM), France.

13

14   **Address of the submitting and corresponding author**

15   Marco Canepari, Laboratoire Interdisciplinaire de Physique (UMR 5588), Bat. E45, 140 avenue de la

16   physique, Domaine univ., 38402 St Martin d'Hères cedex, France. Email: marco.canepari@univ-

17   grenoble-alpes.fr

18

19

20   *Short Title:* Imaging Native Calcium Currents

21

22

23

24

25

26

27

28

29

30

31

32

33

34

35

36

Abstract

Imaging techniques may overcome the limitations of electrode techniques to measure locally not only membrane potential changes, but also ionic currents. Here, we review a recently developed approach to image native neuronal Ca^{2+} currents from brain slices. The technique is based on combined fluorescence recordings using low-affinity Ca^{2+} indicators possibly in combination with voltage sensitive dyes. We illustrate how the kinetics of a Ca^{2+} current can be estimated from the Ca^{2+} fluorescence change and locally correlated with the change of membrane potential, calibrated on an absolute scale, from the voltage fluorescence change. We show some representative measurements from the dendrites of CA1 hippocampal pyramidal neurons, from olfactory bulb mitral cells and from cerebellar Purkinje neurons. We discuss the striking difference in data analysis and interpretation between Ca^{2+} current measurements obtained using classical electrode techniques and the physiological currents obtained using this novel approach. Finally, we show how important is the kinetic information on the native Ca^{2+} current to explore the potential molecular targets of the Ca^{2+} flux from each individual Ca^{2+} channel.

1. Introduction

Optical measurements have been historically designed to monitor the electrical activity of the nervous system, a task where the use of electrode techniques has clear limitations (1). In the last two decades, the development of new organic voltage sensitive dyes (VSD), in parallel with the progress of devices to excite and detect fluorescence (2), allowed optical recordings of sub-cellular membrane potential (V_m) changes < 1 mV with a signal-to-noise ratio (S/N) comparable to that of patch clamp recordings (3). This achievement suggested that voltage imaging can be used to investigate voltage-dependent proteins, in particular voltage-gated ion channels, in their physiological environment. The principal function of an ion channel is to allow an ion flux through a membrane, i.e. to produce an ionic current. Thus, the study of the biophysics of ion channels is routinely performed by measurements of ionic currents in single-electrode or two-electrode voltage clamp (4). A way to investigate the biophysics of isolated native ion channels is to perform excised patches from *ex-vivo* membranes (5). Alternatively, ion channels can be expressed in foreign cells such as oocytes or mammalian cell lines (6) and studied by using patch clamp techniques (7). Yet, the physiological role and function of voltage-gated ion channels must be investigated in their natural environment, i.e. in their native cellular compartment and during physiological changes of V_m. To this purpose, the voltage clamp electrode approach has serious limitations for several reasons. First, the ionic current is measured by maintaining the cell at a given artificial V_m and even if the cell is dynamically clamped the V_m change is never a physiological signal (8). Second, the current measured with the electrode is the summation of the filtered currents from all different cellular regions, including remote regions where V_m is unclamped, and no information is available on the site of origin of the current (9). Third, different ionic currents contribute to the physiological change of V_m producing a functional coupling among the different ion channels (10). Thus, a single native ionic current must be pharmacologically isolated from the total current mediated by the other channels, but the block of these channels will make the V_m change non-physiological.

In the last few years, we designed a novel approach to measure physiological Ca^{2+} currents from neurons in brain slices (11). The method is based on fast Ca^{2+} optical measurements using low-affinity indicators that can be combined with sequential (12) or simultaneous (13) V_m optical recordings. The latter measurements can be calibrated in mV (14) using cell-specific protocols. Individual cells are loaded with Ca^{2+} and V_m indicators using a patch clamp recording. In contrast to voltage-clamp current measurements, the current approach permits independent recordings of the V_m change and of the Ca^{2+} influx, i.e. the study of voltage gating during physiological V_m changes. Since the Ca^{2+} current is reconstructed by the measurement of Ca^{2+} locally binding to an indicator, this approach provides information on channels in different areas of the cell with a spatial resolution as good as the optical recording allows. Finally, the Ca^{2+} current is recorded without blocking all Na^+ and K^+ channels that are necessary to produce the physiological V_m change. The principle of obtaining an optical measurement of a fast Ca^{2+} current is based on the analysis of the dye-Ca^{2+} binding reaction in a cell, a scenario initially studied by Kao and Tsien (15). According to their theoretical estimates

4

116 and to our recent empirical measurements ([16]), the relaxation time of the dye-Ca^{2+} binding reaction is
117 less than 200 µs for low-affinity indicators with equilibrium constant (K_D) ≥ 10 µM such as Oregon
118 Green BAPTA-5N (OG5N, K_D = 35 µM, [17]) or Fura-FF (K_D = 10 µM, [18]). Therefore, a fast Ca^{2+}
119 current with duration of a few milliseconds can be reliably tracked by low-affinity indicators if
120 fluorescence is acquired at sufficiently high speed. The goal of this methodological article is to provide
121 an exhaustive tool for those scientists aiming at performing this type of measurement. The next
122 section addresses in detail the problem of extracting the Ca^{2+} current kinetics from Ca^{2+} fluorescence
123 measurements under different cellular buffering conditions. The following section is devoted to the
124 technical aspects of how to set up combined V_m and Ca^{2+} optical measurements and to calibrate V_m
125 signals on an absolute scale. We then illustrate some examples of combined V_m and Ca^{2+} current
126 measurements and we finally discuss how to correctly interpret the results and how to use this
127 information to significantly advance our knowledge on Ca^{2+} channels function. All data shown here
128 were from experiments performed at the Laboratoire Interdisciplinaire de Physique and approved by
129 the Isere prefecture (Authorisation n. 38 12 01). These experiments were performed at 32-34°C using
130 brain slices from 21-40 postnatal days old C57Bl6 mice of both genders.

131
132

2. Extracting Ca^{2+} current kinetics from Ca^{2+} fluorescence measurements

134

2.1 Biophysical foundations of Ca^{2+} currents imaging

136 An optical measurement of a Ca^{2+} signal is ultimately a measurement of the Ca^{2+} indicator bound
137 to Ca^{2+} ions, which is proportional to the Ca^{2+} fractional change of fluorescence ($\Delta F/F_0$) if the indicator
138 is not saturated. If the kinetics of the Ca^{2+}-binding reaction of the indicator is slower than the kinetics
139 of the Ca^{2+} source, and imaging is performed at higher rate, the time-course of Ca^{2+} $\Delta F/F_0$ essentially
140 tracks the kinetics of the chemical reaction. Alternatively, if the kinetics of the Ca^{2+}-binding reaction is
141 faster than the kinetics of the Ca^{2+} source, the Ca^{2+} $\Delta F/F_0$ signal tracks the kinetics of the Ca^{2+}
142 source. It follows that the equilibration (or relaxation) time of the Ca^{2+}-indicator binding reaction is a
143 crucial variable to use the technique to investigate the biophysics and the physiology of the Ca^{2+}
144 source. The relaxation of the Ca^{2+}- binding reactions for early indicators was studied by Kao and
145 Tsien ([15]) who established that the rate of association for all these molecules is limited by diffusion
146 leading to an association constant of ~$6 \cdot 10^8$ $M^{-1}s^{-1}$. Thus, both the equilibrium constant (K_D) and the
147 equilibrium time are determined by the dissociation constant, i.e. the lower is the affinity of the
148 indicator the shorter is its equilibrium time. We have empirically demonstrated that indicators with K_D ≥
149 10 µM such as OG5N or FuraFF have relaxation time < 200 µs ([16]). Since the kinetics of activation
150 and deactivation of voltage-gated Ca^{2+} channels (VGCCs) during physiological changes of V_m (for
151 instance action potentials), is governed by the kinetics of the V_m transient, it follows that the relaxation
152 time for those indicators is shorter than the duration of the Ca^{2+} influx. Hence, since Ca^{2+} binds to the
153 indicator linearly in time, the Ca^{2+} $\Delta F/F_0$ is proportional to the integral of the Ca^{2+} influx, i.e. to the

integral of the Ca^{2+} current. In the cell, however, Ca^{2+} simultaneously binds to proteins that form the endogenous buffer and this binding is competing with the binding to the indicator. An endogenous buffer can be, in principle, at least as fast as the indicator in equilibrating. In this case, only a fraction of Ca^{2+} is bound to the indicator, but this fraction is proportional to the total Ca^{2+} entering the cell and therefore to the integral of the Ca^{2+} current. Alternatively, an endogenous buffer can equilibrate over a time scale that is longer than the duration of the Ca^{2+} current. In this case, Ca^{2+} first binds to the dye and later to the endogenous buffer, implying that part of Ca^{2+} moves from the indicator to the endogenous buffer during its relaxation time. Under this condition, the Ca^{2+} $\Delta F/F_0$ is not linear with the integral of the Ca^{2+} current over this time scale. To clarify this important concept we make use of two simple computer simulations shown in Fig. 1, produced by a model that takes into account the chemical reactions as well as an extrusion mechanism re-establishing the initial Ca^{2+} conditions over a time scale >100 ms. We analyse what hypothetically can happen if a Ca^{2+} current with Gaussian shape occurs in a cell filled with 2 mM OG5N. In the first simulation (Fig. 1a), the cell has only 1 mM of a fast endogenous buffer behaving with the same association constant of the indicator and K_D = 10 µM. In the second simulation (Fig. 1b), the cell has additional 400 µM of a slower endogenous buffer with association rate ~3 times slower than that of the indicator and K_D = 0.2 µM. In the first case, the time derivative of the Ca^{2+} $\Delta F/F_0$ signal matches the kinetics of the Ca^{2+} current (Fig. 1a). In contrast, in the presence of the slower buffer, the time derivative of the Ca^{2+} $\Delta F/F_0$ signal has a negative component and does not match the kinetics of the Ca^{2+} current (Fig. 1b). In the next two paragraphs, we present the analysis strategies that can be applied to extract the kinetics of Ca^{2+} currents from Ca^{2+} imaging recordings.

2.2 The case of linearity between Ca^{2+} influx and Ca^{2+} fluorescence changes

The proteins expressed in a cell determine whether or not the time course of the Ca^{2+} $\Delta F/F_0$ signal is linear with the kinetics of the Ca^{2+} current. As previously demonstrated (11), in the case of linear behaviour, the Ca^{2+} $\Delta F/F_0$ signal must reach its peak and remain constant for a few milliseconds afterwards, i.e. for the entire duration of the current. As shown in the simulation of Fig. 1a, the kinetics of Ca^{2+} extrusion producing a slow decrease of the Ca^{2+} $\Delta F/F_0$ signal has negligible effect on the time derivative. Thus, the estimate of the Ca^{2+} current kinetics is reliably obtained by the calculation of the time derivative of the Ca^{2+} $\Delta F/F_0$ signal. This calculation, however, requires the signal noise to be smaller than the signal change between two consecutive samples. The classical way to achieve this necessary condition is to apply to the Ca^{2+} $\Delta F/F_0$ signal a "smoothing algorithm", i.e. a temporal filter that reduces the noise of the signal with minimal distortion of its kinetics. At 20 kHz acquisition rate, we have found that the Savitky-Golay algorithm (19) is an optimal filtering tool permitting noise reduction of the signal without significant temporal distortion using time-windows of up to 20-30 samples (11). The applicability of this strategy has however limitations, i.e. if the signal or the region of measurement are too small, or if the light is too dim, the smoothing of the signal might not be sufficient to reduce the noise down to the level permitting calculation of the time derivative. In this

192   case, the alternative strategy to apply consists in fitting the raw or the filtered Ca^{2+} $\Delta F/F_0$ signal with a

193   model function obtaining a noiseless curve that mimics the time course of the Ca^{2+} $\Delta F/F_0$ signal. A

194   simple choice of function that resembles the time course of the Ca^{2+} $\Delta F/F_0$ transient is the sigmoid. In

195   particular, we found that the product of three sigmoid functions always provides an excellent fit of the

196   Ca^{2+} $\Delta F/F_0$ signal associated with a backpropagating action potential in CA1 hippocampal pyramidal

197   neurons (16). As shown in the example of Fig. 2a both strategies are faithful in correctly calculating

198   the time derivative of the $\Delta F/F_0$ signal. In this example, a CA1 hippocampal pyramidal neuron was

199   filled with 2 mM OG5N and the dendritic Ca^{2+} $\Delta F/F_0$ signal associated with a backpropagating action

200   potential was recorded at 20 kHz and averaged over 16 trials. This high sampling frequency was

201   necessary to avoid signal aliasing and therefore distortion of the kinetics of the current. The filtering

202   strategy is the straightforward approach that enables the calculation of the time derivative, but it

203   produces a curve with noise. The noise can be reduced (if possible) by increasing the number of trials

204   to average or by enlarging the dendritic area from where fluorescence is averaged. The fitting strategy

205   is less direct but it produces a noiseless curve and it is therefore the only possible approach when the

206   noise of the Ca^{2+} $\Delta F/F_0$ signal is above a certain level, as quantitatively estimated in an original report

207   (16). In particular, this is the case when the current must be extracted from single trials or when the

208   recording is obtained from small or relatively dim regions.

209

210 2.3 The case of nonlinearity between Ca^{2+} influx and Ca^{2+} fluorescence changes

211   The method of estimating the kinetics of a Ca^{2+} current by calculating the Ca^{2+} $\Delta F/F_0$ time

212   derivative fails when Ca^{2+} unbinds from the indicator over a time scale that is longer than the current

213   duration, but sufficiently short to distort the estimate of Ca^{2+} influx dynamics by fluorescence

214   measurement. In other words, this method fails when the Ca^{2+} $\Delta F/F_0$ signal decays rapidly, after

215   correction for bleaching, generating a negative component in its time derivative. Such a situation

216   occurs, for example, where slow buffering is produced by Calbindin-D28k (20,21) and Parvalbumin

217   (22,23). As shown in the example of Fig. 2b, the Ca^{2+} $\Delta F/F_0$ signal associated with a climbing fibre

218   excitatory postsynaptic potential (EPSP), recorded at 5 kHz from a dendritic region and averaged over

219   four trials, decays rapidly after its maximum resulting in a negative component of its time derivative.

220   The distortion from the linear behaviour produced by the slow buffers can be compensated by taking

221   into account the kinetics of Ca^{2+} unbinding from the indicator. We have recently developed a

222   successful method to achieve this goal (24). The strategy is based on fitting the decay time of the

223   Ca^{2+} $\Delta F/F_0$ signal with the result of a computer simulation of a model with a slow buffer. Initially the

224   input current is the Gaussian function fitting the rising phase of the time derivative (that is still a good

225   approximation of the initial part of the current). The kinetic parameters and the concentration of the

226   slow buffer are set to obtain the best fit of the decay phase of the Ca^{2+} $\Delta F/F_0$ signal. Then, the kinetics

227   of the Ca^{2+} current is obtained as summation of four Gaussian functions that maximise the match

228   between the result of the computer simulation and the experimental Ca^{2+} $\Delta F/F_0$ signal. Although this

229   new method provides only an indirect approximation of the kinetics of the Ca^{2+} current, this

information is crucial at understanding the activation and deactivation of different types of VGCCs. In the dendrites of PNs, for instance, different Ca^{2+} current kinetics components are associated with the activation of P/Q-type VGCCs (25) and T-type Ca^{2+} channels (26) that can be in principle separated by pharmacological block of one component. Thus, the extrapolation of a curve that approaches the kinetics of the Ca^{2+} current can be used to quantitatively investigate the variability of channels activation at different dendritic sites, the modulation of channel activation due to physiological activity or to pharmacological action. Finally, it is important to say that such a strategy can be extended to estimate slower Ca^{2+} currents where the fitting procedure can be applied to the slower decay time due to Ca^{2+} extrusion (27).

3. Combining membrane potential and Ca^{2+} Imaging

3.1 Setting up combined voltage and Ca^{2+} fluorescence measurements

To combine V_m and Ca^{2+} optical measurements, the VSD and the Ca^{2+} indicator must have minimal overlap in the emission spectra. Water soluble voltage indicators with different excitation and emission spectra have been recently developed (28). In particular, the red-excitable and IR emitting VSD ANBDQPTEA (or PY3283) is suitable for coupling with other optical techniques (29). Nevertheless, the most used VSDs for single cell applications are still JPW3028 (30) and the commercially available JPW1114 (18). These indicators have wide excitation spectrum in the blue/green region and they emit mainly in the red region. We have previously demonstrated that both indicators can be optimally combined with Fura indicators that are excited in the UV region and emit in the short green region (12). In this case, VSDs were excited at 543 nm using a laser and Fura indicators were excited at 385 nm using a light emitting diode (LED) as shown in the scheme of Fig.3a. Alternatively, simultaneous voltage and Ca^{2+} imaging can be achieved using Oregon Green, Calcium Green or Fluo Ca^{2+} indicators using blue light (470 – 490 nm) to excite both VSDs and Ca^{2+} indicators (31). Simultaneous imaging of JPW1114 and Oregon Green BAPTA-5N (OG5N) was adopted to obtain the first combined measurement of V_m and Ca^{2+} currents using the configuration of Fig.3b. This type of measurement, however, has several disadvantages. First, OG5N fluorescence has a small tail component in the red region (31) which can be negligible or not depending on the ratio of the two dyes at each site as well as on the ratio between the two signals. Thus, for example, it works in proximal dendrites of CA1 pyramidal neurons for signals associated with action potentials (11), where V_m fluorescence is stronger than Ca^{2+} fluorescence, but it does not in distal dendrites of cerebellar Purkinje neurons (PNs, data not shown), where V_m fluorescence is weaker than Ca^{2+} fluorescence. A second disadvantage is that the JPW1114 signal at 470 nm excitation is ~4 times smaller than that at 532 nm excitation. If simultaneous recordings are not critical, one can replace them with sequential recordings obtained by alternating 470 nm and 532 nm excitation as used in a recent study (32). Finally, a third disadvantage is that JPW1114 absorbs more in the blue range than

in the green range, i.e. it exhibits toxic effects after fewer exposures. A crucial technical aspect to take into consideration while setting up combined voltage and Ca^{2+} fluorescence measurements is the ability to record the two signals simultaneously at high speed. To this purpose, the company RedShirtImaging (Decantur, GA) has developed a dual-head version of the SMQ NeuroCCD (Fig. 3c). This camera permits simultaneous image acquisitions from both heads at 5-20 kHz, i.e. at the required speed. A demagnifier developed by Cairn Research Ltd (Faversham, UK) allows adjusting the size of the image before it is split in two images at the emission wavelengths of the two dyes. Thus, the alignment of the two heads of the camera allows obtaining, at each precise region of interest, the V_m and the Ca^{2+} signal.

2.2 Calibrating membrane potential fluorescence transients

The calibration of V_m optical signals on an absolute scale (in mV) is crucial to analyse the gating of Ca^{2+} channels at the same locations where Ca^{2+} recordings are performed. This is not, however, straightforward. Indeed, the fractional change of VSD fluorescence is proportional to V_m (33), but the linear coefficient between these two quantities depends on the ratio between the inactive dye and the active dye that varies from site to site. The inactive dye is bound to membranes that do not change potential and contributes only to the resting fluorescence, while the active dye is bound to the plasma membrane and contributes to the resting fluorescence, but also carries the signal. In particular, in experiments utilising intracellular application of the dye, inactive dye is the dye that binds to intracellular membranes and organelles. Since the sensitivity of recording varies from site to site, a calibration can be achieved only if a calibrating electrical signal that has known amplitude at all locations is available. Such a signal is different in different systems. In mitral cells of the olfactory bulb, the amplitude of an action potential is the same in the whole apical dendrite and it can be used to create a sensitivity profile of the measuring system (34). Another type of calibrating electrical signal can be a slow electrical change spreading with minimal attenuation over relatively long distances. Such a signal can be used to reliably calibrate VSD signals in PNs (18). An example of this type of calibration is reported in Fig. 4a. Starting from the resting V_m, that we assume nearly uniform over the entire cell, long current hyperpolarising or depolarising current pulses are injected to the soma *via* the patch pipette and the change in V_m is recorded. As shown by direct dendritic patch recording, the dendrite is hyperpolarised by the same amount of the soma (35). Thus, the measurement of somatic hyperpolarisation can be used as voltage reference to calibrate the dendritic VSD fractional change of fluorescence (VSD $\Delta F/F_0$) optical signal, as shown in Fig. 4a. In contrast, a depolarisation step attenuates along the dendrite. A third type of calibrating signal is a uniform depolarisation over the entire dendritic tree using L-glutamate photolysis from 4-Methoxy-7-nitroindolinyl-caged-L-glutamate (MNI-glutamate) (14). This calibration procedure is applicable to all membrane expressing a relatively large number of glutamate receptors, i.e. to dendrites with high densities of excitatory synapses. The calibration is based on the principle that if the ionotropic glutamate receptor becomes the dominant conductance in a particular neuronal compartment, its reversal potential will determine the membrane

potential of the compartment. Thus, in the area where dominance of glutamate receptor conductance is obtained, the resulting V_m change will be the same and can be used to calibrate VSD signals. An example of this protocol to calibrate backpropagating action potentials in CA1 hippocampal pyramidal neurons is shown in Fig. 4b. The VSD $\Delta F/F_0$ signal associated with the backpropagating AP at different sites of the apical dendrites is variable and cannot be directly correlated with the absolute change of V_m. In the presence of 1 μM TTX, to block action potentials, L-glutamate is photoreleased to saturate glutamate receptors over the whole field of view. Since the recording is performed starting from the resting V_m, the size of the VSD $\Delta F/F_0$ corresponds to this potential in the whole illuminated area where V_m reaches the reversal potential of 0 mV. Thus, this information is used to extrapolate the V_m at each dendritic site.

4. Examples of combined voltage and Ca^{2+} current imaging

4.1 Ca^{2+} currents associated with backpropagating action potentials in CA1 hippocampal pyramidal neurons and in olfactory bulb mitral cells

In many neurons, action potentials generated in the axon hillock adjacent to the soma do not only propagate along the axon to reach neurotransmitter release terminals, but also backpropagate throughout dendrites to signal cell activation at the sites where the neuron receives the synaptic inputs. At least part of this information is given by the fast Ca^{2+} transients produced by activation of VGCCs caused by the dendritic depolarisation associated with the action potential. The analysis that can be performed using the present imaging method is therefore crucial at understanding signal processing in individual neurons, as well as the specific role and function of the diverse VGCCs activated in dendrites. The propagation of the action potential and the consequent activation of VGCCs may be very different in different neuronal systems. In CA1 hippocampal pyramidal neurons, action potentials attenuate along the dendrite and activate both high-voltage activated (HVA) and low-voltage activated (LVA) VGCCs (36, 37). We have very recently demonstrated that HVA-VGCCs and LVA-VGCCs operate synergistically to stabilise Ca^{2+} signals during burst firing (32). Somatic and dendritic action potentials, at nearly physiological temperature, have 1-4 ms duration as in the example shown in Fig. 5a. In agreement with this, the kinetics of the Ca^{2+} current is similar to that of the action potential, with a peak delayed by a few hundred milliseconds from the peak of the action potential. In total contrast to the CA1 hippocampal pyramidal neuron, in olfactory bulb mitral cells the action potential does not attenuate along the dendrites (38). In addition, as shown in the representative example of Fig. 5b, the somatic and dendritic action potential at near physiological temperature (32-34 °C) has duration < 1 ms. Thus, in this system, the activation and deactivation of VGCCs is also faster leading to a Ca^{2+} current with shorter duration and shorter delay from the V_m waveform peak. This preliminary comparison between the two cases indicates that the role of VGCCs, activated by the action potential, is different in different systems. For example, Ca^{2+} currents

344   with delays of ~100 µs in presynaptic terminal where the function of this signal is to trigger

345   neurotransmitter release (39). Here, the kinetics of the Ca^{2+} current was obtained by calculating the

346   time derivative of the Ca^{2+} $\Delta F/F_0$ signal fit (16). VGCCs contribute to the shape of the action potential

347   directly and indirectly by activating K^+ channels, but also provide a precise time-locked Ca^{2+} transient

348   capable to select fast-activated Ca^{2+} binding proteins. The possibility to locally investigate, using

349   combined V_m and Ca^{2+} current optical measurements, the physiological occurrence of Ca^{2+} signals

350   mediated by VGCCs will contribute enormously, in the near future, to the understanding of complex

351   signal processing in neurons.

352

4.2 Ca^{2+} currents associated with climbing fibre EPSPs in cerebellar Purkinje neurons

354   In contrast to pyramidal neurons of the cortex and hippocampus, and to olfactory bulb mitral cells,

355   somatic/axonal action potentials in PNs do not actively propagate in the dendrites (40). The dendrites

356   of PNs, however, express P/Q-type HVA-VGCCs (25) and T-type LVA-VGCCs (26) that are activated

357   by the dendritic depolarisation produced by climbing fibre EPSPs. As shown in the example of Fig. 6,

358   the shape of the dendritic V_m, calibrated in Fig. 4a is quite different in the soma and in the dendrite,

359   mainly reflecting the absence of Na^+ action potentials in the dendrite. In this system, the low-affinity

360   Ca^{2+} indicator used to estimate the Ca^{2+} current was Fura-FF, since the larger Ca^{2+} signal produced

361   by OG5N contaminated the optical V_m measurement. The prominent dendritic depolarisation

362   produces a biphasic Ca^{2+} current, which is in this case obtained by applying our recent generalised

363   method (24). The fast and sharp component is nearly concomitant to the short period in which V_m > -

364   40 mV and it is therefore likely mediated by HVA-VGCCs. The slower and more persistent component

365   is instead mostly concomitant to the whole depolarisation transient and is therefore likely mediated by

366   LVA-VGCCs, as demonstrated by selectively blocking T-type VGCCs (unpublished data not shown).

367   The analysis of Ca^{2+} signalling associated with the climbing fibre EPSP is crucial for the

368   understanding of synaptic plasticity in PNs (41). Yet, while the role of the Ca^{2+} transient associated

369   with the climbing fibre EPSP has been postulated to be auxiliary to the principal Ca^{2+} signal mediated

370   by parallel fibre EPSPs, these first measurements of the Ca^{2+} current kinetics elucidate a quite

371   precise timing of occurrence of the Ca^{2+} source that may eventually provide a less ambiguous

372   explanation of the precise function of this spread dendritic depolarisation. In summary, the examples

373   illustrated in this section show the potentials of this novel optical method in providing physiological

374   information not available by using electrode techniques.

375

376

5. Data interpretation and future prospective

378

379   The method described here has been developed to overcome the limitations of single-electrode

380   or two-electrode voltage clamp techniques permitting the analysis of physiological Ca^{2+} currents of

381   native Ca^{2+} channels. Indeed, in contrast to patch-clamp recordings, these Ca^{2+} optical currents can

382 be measured in conditions of a physiological change of V_m and the measured currents are confined to

383 the sites where they are recorded, as shown in apical dendrites of hippocampal pyramidal neurons

384 (32). The additional information on local V_m change, necessary to correlate the behaviour of the

385 conductance with its biophysical properties, is obtained by combining VSD imaging. In cases of linear

386 behaviour between Ca^{2+} influx and Ca^{2+} fluorescence changes the kinetics of the Ca^{2+} current can be

387 extracted by calculating the time derivative of the Ca^{2+} $\Delta F/F_0$ signal using low-affinity Ca^{2+} indicators

388 (11, 16). In the case of nonlinear behaviour between Ca^{2+} influx and Ca^{2+} fluorescence, produced by

389 Ca^{2+}-binding proteins with slower kinetics with respect to the Ca^{2+} current, the kinetics of the Ca^{2+}

390 current can be still correctly estimated by taking into account the faster unbinding of Ca^{2+} from the

391 low-affinity indicator (24). In this last section we address the question of how data, obtained using this

392 technique, should be interpreted. In Ca^{2+} current recordings from channels expressed in heterologous

393 systems using voltage clamp, V_m is controlled artificially and its change is therefore independent of

394 the channel deactivation. Under physiological conditions, Ca^{2+} channels contribute to the V_m change

395 directly, through the ion flux, and indirectly by regulating other conductances. It follows that the

396 channel deactivation changes the V_m waveform. We have shown that in CA1 hippocampal pyramidal

397 neurons this phenomenon produces a modulation of LVA-VGCCs by HVA-VGCCs (32). More in

398 general, a Ca^{2+} current mediated by diverse VGCCs is always the result of a synergy among all

399 different ion channels contributing to the V_m waveform. It follows that in a Ca^{2+} current optical

400 measurement, a single component of the current cannot be extracted simply by blocking the

401 underlying channel, since this block may affect the residual current as well. This evidence has

402 important implications in the study of transgenic animals carrying Ca^{2+} channel mutations. In this

403 case, a certain phenotype is likely to result from the combined modification of function of many

404 different channels, rather than from the specific Ca^{2+} influx component, making the study of these

405 animals as models for disease challenging. In summary, the investigation of the role and function of

406 individual Ca^{2+} channels must be performed in the global context of activation of all channels

407 participating to the local V_m waveform.

408 Another important aspect of data interpretation is the relation of the kinetics of Ca^{2+} current with

409 the putative molecular targets of Ca^{2+} ions entering the cell. While importance is normally given to

410 possible molecular coupling between the Ca^{2+} channel and the Ca^{2+} binding protein, the kinetics of

411 the Ca^{2+} current can be a potent selector of the molecular pathway which is activated. To illustrate this

412 important concept we make use of computer simulations using the same theoretical framework for

413 simple Ca^{2+}-binding dynamics that we already used in the past (42). We imagine the possible

414 activation of two proteins: a "fast" protein with $K_{ON} = 5.7 \cdot 10^8$ $M^{-1}s^{-1}$ and $K_D = 10$ µM, expressed at the

415 concentration of 500 µM; and a "slow" protein with $K_{ON} = 4 \cdot 10^8$ $M^{-1}s^{-1}$ and $K_D = 0.4$ µM, expressed at

416 the concentration of 100 µM. In the first case, shown in Fig. 7a, the cell is receiving a fast Ca^{2+} current

417 with ~ 2 ms total duration which binds first to the fast protein and later to the slow protein. In the

418 second case, shown in Fig. 7b, the cell is receiving a slower Ca^{2+} current that is smaller in amplitude

419 but that carries approximately the same amount of Ca^{2+}. In this case the slow protein binds to Ca^{2+}

420 with a slower kinetics but the amount of the fast protein binding to Ca^{2+} is less than half with respect

421 to the first case. These simulations indicate that the ability to activate for a molecular pathway
422 triggered by the fast protein strongly depends on the kinetics of the Ca^{2+} current. Thus, the approach
423 described here should drastically improve our understanding of the physiological function of Ca^{2+}
424 channels by providing the possibility to explore the biophysics of native channels during physiological
425 activity locally within the complex neuronal architecture. The examples of combined V_m and Ca^{2+}
426 current optical measurements from CA1 hippocampal pyramidal neurons, olfactory bulb mitral cells
427 and PNs reported here are representative of the types of exploration that can be performed using this
428 novel approach.

References

[1] Braubach O, Cohen LB, Choi Y (2015) Historical Overview and General Methods of Membrane Potential Imaging. Adv Exp Med Biol 859: 3-26

[2] Davies R, Graham J, Canepari M (2013) Light sources and cameras for standard in vitro membrane potential and high-speed ion imaging. J Microsc 251: 5-13

[3] Canepari M, Willadt S, Zecevic D, Vogt KE (2010) Imaging Inhibitory Synaptic Potentials Using Voltage Sensitive Dyes. Biophys J 98: 2032-2040

[4] Sakmann, B, Neher E (1986) Patch clamp techniques for studying ionic channels in excitable membranes. Annu Rev Physiol 46: 455-472

[5] Gray R, Johnston D (1985) Rectification of single GABA-gated chloride channels in adult hippocampal neurons. J Neurophysiol 54: 134-142

[6] Lester HA (1988) Heterologous expression of excitability proteins: route to more specific drugs? Science 241: 1057-1063

|7] Guy HR, Conti F (1990) Pursuing the structure and function of voltage-gated channels. Trends Neurosci 13: 201-206

[8] Antic SD (2016) Simultaneous recordings of voltage and current waveforms from dendrites. J Physiol 594: 2557-2558.

[9] Williams SR, Mitchell SJ (2008) Direct measurement of somatic voltage clamp errors in central neurons. Nat Neurosci 11: 790-798.

459 [10] Hodgkin AL, Huxley AF (1952) Currents carried by sodium and potassium ions through the
460   membrane of the giant axon of Loligo. J Physiol 116: 449-472.

461 [11] Jaafari N, De Waard M, Canepari M (2014) Imaging Fast Calcium Currents beyond the
462   Limitations of Electrode Techniques. Biophys J 107: 1280-1288

463 [12] Canepari M, Vogt K, Zecevic D (2008) Combining voltage and calcium imaging from neuronal
464   dendrites. Cell Mol Neurobiol 58: 1079-1093

465 [13] Vogt KE, Gerharz S, Graham J, Canepari M (2011a) High-resolution simultaneous voltage and
466   Ca^{2+} imaging. J Physiol 589: 489-494

467 [14] Vogt KE, Gerharz S, Graham J, Canepari M (2011b) Combining membrane potential imaging
468   with L-glutamate or GABA photorelease. PLoS ONE 6: e24911

469 [15] Kao JP, Tsien RY (1988) Ca2+ binding kinetics of fura-2 and azo-1 from temperature-jump
470   relaxation measurements. Biophys J 53: 635-639

471 [16] Jaafari N, Marret E, Canepari M (2015) Using simultaneous voltage and calcium imaging to study
472   fast Ca2+ channels. Neurophotonics 2: 021010

473 [17] Canepari M, Odgen D (2006) Kinetic, pharmacological and activity-dependent separation of two
474   Ca^{2+} signalling pathways mediated by type 1 metabotropic glutamate receptors in rat Purkinje
475   neurons. J Physiol 573: 65-82

476 [18] Canepari M, Vogt, KE (2008) Dendritic Spike Saturation of Endogenous Calcium Buffer and
477   Induction of Postsynaptic Cerebellar LTP. PLoS ONE 3: e4011

478 [19] Savitzky A, Golay MJE (1964) Smoothing and Differentiation of Data by Simplified Least Squares
479   Procedures. Anal Chem 36: 1627-1639

480 [20] Nägerl UV, Novo D, Mody I, Vergara JL (2000) Binding kinetics of calbindin-D(28k) determined
481   by flash photolysis of caged Ca(2+). Biophys J 79: 3009-3018

482 [21] Airaksinen MS, Eilers J, Garaschuk O, Thoenen H, Konnerth A, Meyer M (1997) Ataxia and
483   altered dendritic calcium signalling in mice carrying a targeted nullmutation of the calbindin
484   D28k gene. Proc Natl Acad Sci USA 94: 1488-1493

485 [22] Lee SH, Schwaller B, Neher E (2000) Kinetics of Ca2+ binding to parvalbumin in bovine
486   chromaffin cells: implications for [Ca2+] transients of neuronal dendrites. J Physiol 525: 419-
487   432

488 [23] Schmidt H, Stiefel KM, Racay P, Schwaller B, Eilers J (2003) Mutational analysis of dendritic
489   Ca2+ kinetics in rodent Purkinje cells: role of parvalbumin and calbindin D28k. J Physiol 551:
490   13-32

491 [24] Ait Ouares K, Jaafari N, Canepari M (2016) A generalised method to estimate the kinetics of fast
492   Ca^{2+} currents from Ca^{2+} imaging experiments. J Neurosci Methods 268: 66-77

493 [25] Usowicz MM, Sugimori M, Cherksey B, Llinás R (1992) P-type calcium channels in the somata
494   and dendrites of adult cerebellar Purkinje cells. Neuron 9: 1185-1199

495 [26] Isope P, Hildebrand ME, Snutch TP (2012) Contributions of T-type voltage-
496   gated calcium channels to postsynaptic calcium signaling within Purkinje neurons. Cerebellum
497   11: 651-665

498 [27] Miyakawa H, Lev-Ram V, Lasser-Ross N, Ross WN (1992) Calcium transients evoked by
499   climbing fiber and parallel fiber synaptic inputs in guinea pig cerebellar Purkinje neurons. J
500   Neurophysiol 68: 1178-1189

501 [28] Yan P, Acker CD, Zhou WL, Lee P, Bollensdorff C, Negrean A, Lotti J, Sacconi L, Antic SD, Kohl
502   P, Mansvelder HD, Pavone FS, Loew LM (2012) Palette of fluorinated voltage-sensitive
503   hemicyanine dyes. Proc Natl Acad Sci USA 109: 20443-20448

504 [29] Willadt S, Canepari M, Yan P, Loew LM, Vogt KE (2014) Combined optogenetics and voltage
505   sensitive dye imaging at single cell resolution. Front Cell Neurosci 8: 311

506 [30] Antic SD (2003) Action potentials in basal and oblique dendrites of rat neocortical pyramidal
507   neurons. J Physiol 550: 35-50

508 [31] Bullen A, Saggau P (1998) Indicators and optical configuration for simultaneous high-resolution
509   recording of membrane potential and intracellular calcium using laser scanning microscopy.
510   Pflügers Arch 436: 788–796

511 [32] Jaafari N, Canepari M (2016) Functional coupling of diverse voltage-gated Ca(2+) channels
512   underlies high fidelity of fast dendritic Ca(2+) signals during burst firing. J Physiol 594: 967-
513   983

514 [33] Loew LM, Simpson LL (1981) Charge-shift probes of membrane potential: a probable
515   electrochromic mechanism for p-aminostyrylpyridinium probes on a hemispherical lipid bilayer.
516   Biophys J 34: 353-365

517 [34] Djurisic M, Antic S, Chen WR, Zecevic D (2004) Voltage imaging from dendrites of mitral cells:
518   EPSP attenuation and spike trigger zones. J Neurosci 24: 6703-6714

519 [35] Roth A, Häusser M (2001) Compartmental models of rat cerebellar Purkinje cells based on
520   simultaneous somatic and dendritic patch-clamp recordings. J Physiol 535: 445-472

521 [36] Spruston N, Schiller Y, Stuart G, Sakmann B (1995) Activity-dependent action potential invasion
522   and calcium influx into hippocampal CA1 dendrites. Science 268: 297-300

523 [37] Canepari M, Djurisic M, Zecevic D (2007) Dendritic signals from rat hippocampal CA1 pyramidal
524   neurons during coincident pre- and post-synaptic activity: a combined voltage- and calcium-
525   imaging study. J Physiol 580: 463-484

526 [38] Bischofberger J, Jonas P (1997) Action potential propagation into the presynaptic dendrites of
527   rat mitral cells. J Physiol 504: 359-365

528 [39] Sabatini BL, Regerh WG (1996) Timing of neurotransmission at fast synapses in the mammalian
529   brain. Nature 384: 170-172.

530 [40] Stuart G, Häusser M (1994) Initiation and spread of sodium action potentials in cerebellar
531   Purkinje cells. Neuron 13: 703-712

532 [41] Vogt KE, Canepari M (2010) On the induction of postsynaptic granule cell-Purkinje neuron LTP
533   and LTD. Cerebellum 9: 284-290

534 [42] Canepari M, Mammano F (1999) Imaging neuronal calcium fluorescence at high spatio-temporal
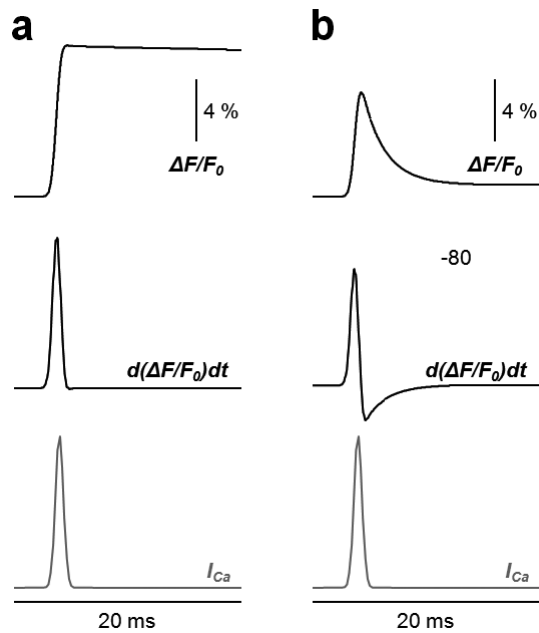535   resolution. J. Neurosci. Methods 1999; 87:1 -11

536

Fig. 1. Simulation of hypothetical Ca^{2+} $\Delta F/F_0$ signals from 2 mM OG5N in the presence of endogenous Ca^{2+} buffers. (**a**) Simulation of $\Delta F/F_0$ signal (top trace) following a Ca^{2+} current with simple Gaussian kinetics (I_{Ca}, gray trace on the bottom) in the presence of 1 mM of a fast endogenous Ca^{2+} buffer with same association constant of the Ca^{2+} indicator ($5.7 \cdot 10^8$ $M^{-1}s^{-1}$) and $K_D = 10$ μM. The kinetics of the $\Delta F/F_0$ time derivative (middle trace) matches the kinetics of the Ca^{2+} current. (**b**) Same as in the previous panel but in this case in the presence of additional 400 μM of a slower buffer with association constant equal to $2 \cdot 10^8$ $M^{-1}s^{-1}$ and $K_D = 0.2$ μM. The kinetics of the $\Delta F/F_0$ time derivative (middle trace) does not matches the kinetics of the Ca^{2+} current.

537

538
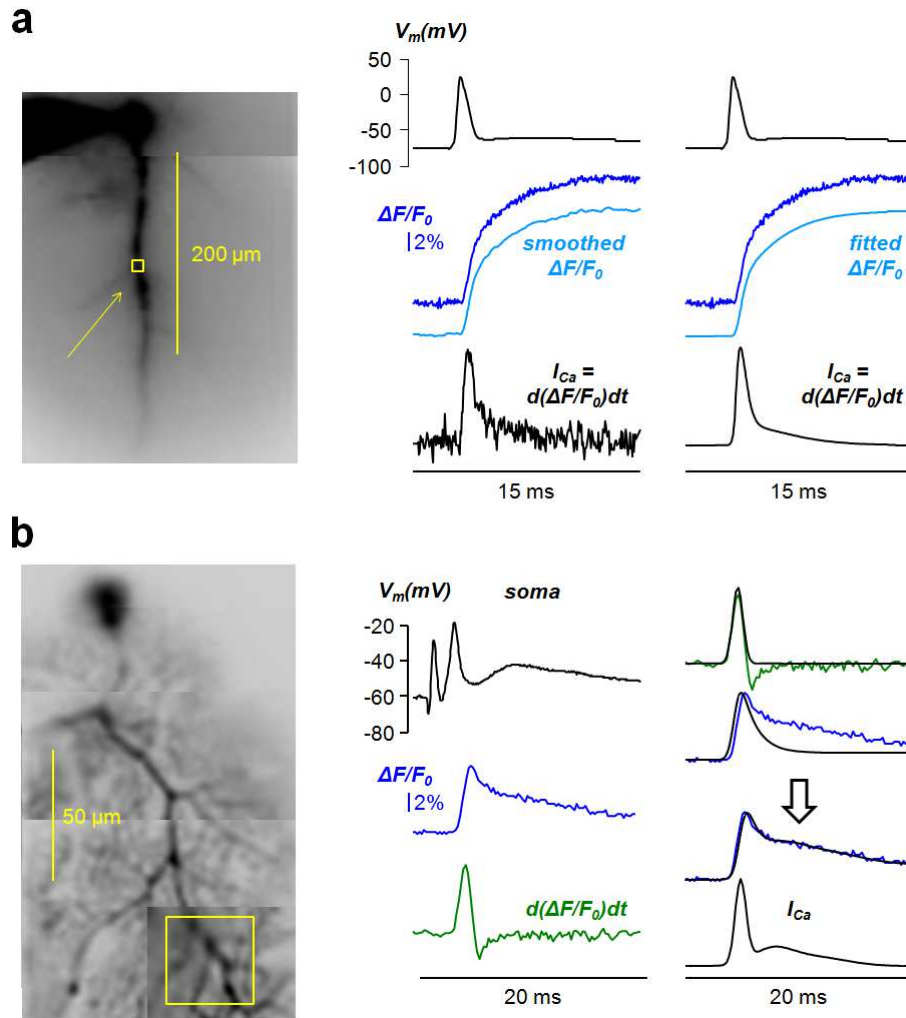
539

540 Fig. 2. Different strategies to estimate the kinetics of a Ca^{2+} current (**a**) On the left, fluorescence
541 image of CA1 hippocampal pyramidal neuron filled with 2 mM OG5N with a small region of the apical
542 dendrite outlined and indicated by the arrow. On the right, somatic V_m change associated with an
543 action potential (top black traces) and Ca^{2+} $\Delta F/F_0$ signal in the indicated region (blue trace). The $\Delta F/F_0$
544 signal is either smoothed with a Savitky-Golay algorithm (left) or fitted with a 3-sigmoid function
545 (right). The Ca^{2+} current kinetics (I_{Ca}) is then estimated by calculating the time derivative of the
546 processed $\Delta F/F_0$ signal. The kinetics of the current is the same using the two strategies, but the curve
547 obtained with the strategy of data fitting is noiseless. Data, recorded at 20 kHz, were from averages of
548 16 trials. (**b**) On the left, fluorescence image of PN filled with 2 mM OG5N with square region of
549 interest outlined. On the right, somatic V_m change associated with a climbing fibre EPSP (top-left
550 black trace) and Ca^{2+} $\Delta F/F_0$ signal in the indicated region (blue traces). The time derivative of the Ca^{2+}
551 $\Delta F/F_0$ signal (green traces) does not match the kinetics of the current. To estimate the kinetics of the
552 current we use a strategy that consists in matching the result of a computer simulation to the Ca^{2+}
553 $\Delta F/F_0$ signal using an optimised two-buffer model (24). We start from the Gaussian function fitting the
554 rising phase of the $\Delta F/F_0$ time derivative (top-right black trace). We then correct the current with three
555 additional Gaussian components until a match of the computer simulation with the Ca^{2+} $\Delta F/F_0$ signal
556 is obtained (process indicated by the arrow. The curve producing this match (I_{Ca}, bottom-right black

17

557 trace) is the estimate of the Ca^{2+} current kinetics. Data, recorded at 5 kHz, were from averages of 4

558 trials.

559

560
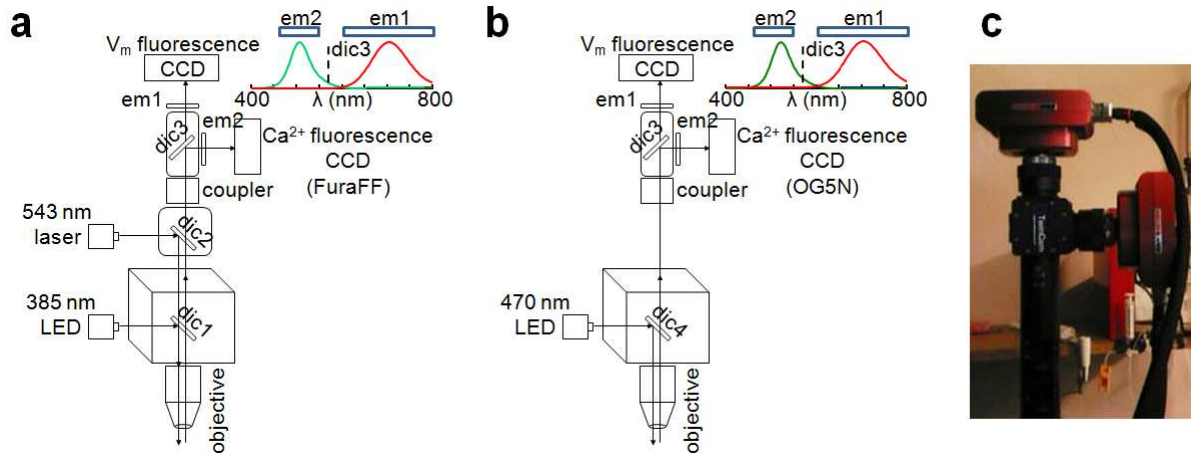
561

562 Fig. 3. Configurations and camera for combined voltage and Ca^{2+} fluorescence measurements. (**a**)

563 Schematic drawing of the apparatus for simultaneous voltage and Ca^{2+} imaging using the VSD

564 JPW1114 and the Ca^{2+} indicator FuraFF ([13]); 385 nm LED light via the epifluorescence port of a

565 commercial microscope is reflected by a 506 nm long-pass dichroic mirror (dic1); 543 nm laser light

566 via the top of the microscope is reflected by a dual-band dichroic mirror transmitting wavelengths

567 between 493 nm and 530 nm and wavelengths longer than 574 nm (dic2); the fluorescence images of

568 the two dyes are demagnified and separated by a 565 nm long-pass dichroic mirror (dic3); The V$_m$

569 image and the Ca^{2+} images are filtered by a 610 nm long-pass (em1) and by a 510±42 nm band-pass

570 filter (em2) respectively, then acquired by two CCD cameras; the emission spectra of FuraFF (green)

571 and JPW1114 (red) are shown on the top-right. (**b**) Schematic drawing of the apparatus for

572 simultaneous voltage and Ca^{2+} imaging using the VSD JPW1114 and the Ca^{2+} indicator OG5N ([11]);

573 470 nm LED light via the epifluorescence port of a commercial microscope is reflected by a 495 nm

574 long-pass dichroic mirror (dic4); the fluorescence images of the two dyes are demagnified and and

575 processed as in the previous configuration; the emission spectra of OG5N (green) and JPW1114

576 (red) are shown on the top-right. (**c**) The dual NeuroCCD camera designed by RedshirtImaging for

577 this type of measurement.
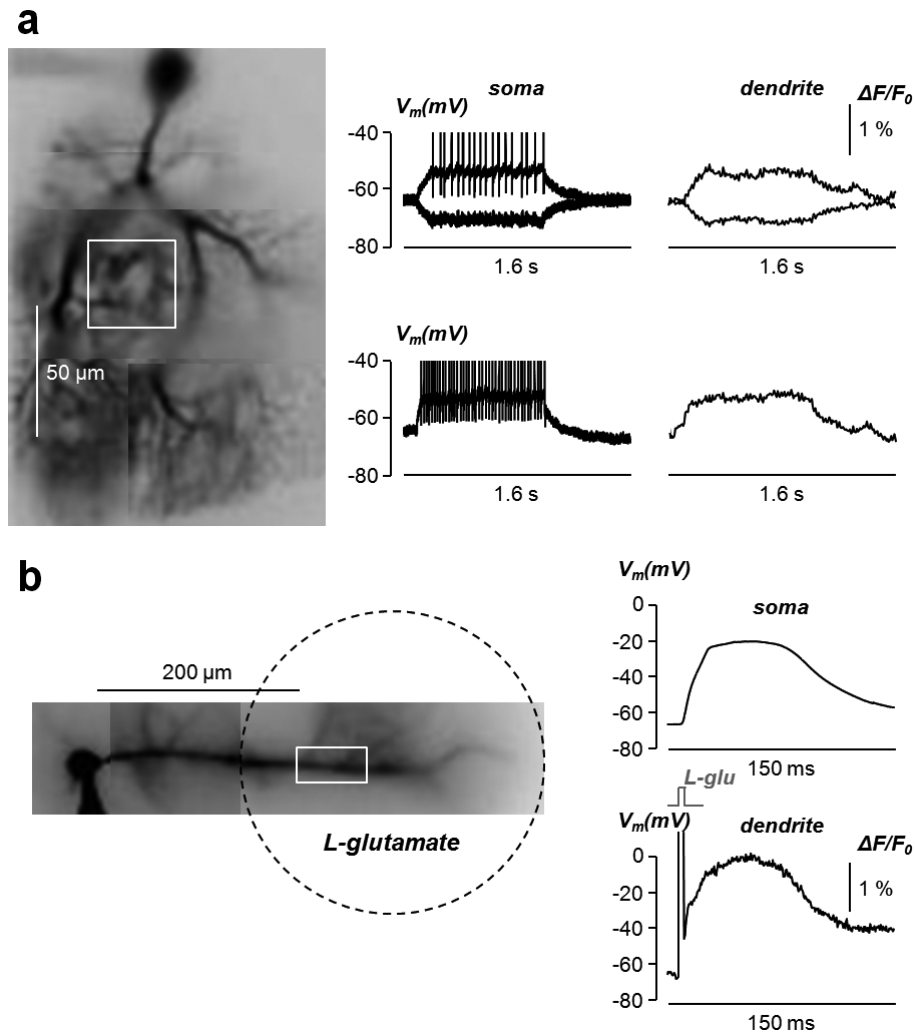
Fig. 4. Calibration methods for dendritic V_m optical signals. (**a**) On the left, fluorescence image of PN with square region of interest outlined. On the right, somatic V_m change associated with long hyperpolarising or depolarising steps and associated dendritic VSD $\Delta F/F_0$ signals in the region of interest; the hyperpolarising step spreads to the dendrites with negligible attenuation (35) and is used to calibrate the VSD $\Delta F/F_0$ signals; the weak depolarising step on the top also spreads with minimal attenuation, but the associated somatic action potentials do not propagate into the dendrites; in contrast, the strong depolarising step on the bottom attenuates. (**b**) On the left, fluorescence image of CA1 hippocampal pyramidal neuron with rectangular region, 200-250 µm from the soma, outlined. On the right, somatic V_m change associated with L-glutamate photorelease from MNI-glutamate (14) in the area limited by the dotted line and in the presence of 1 µM tetrodotoxin blocking action potentials; the dendritic VSD $\Delta F/F_0$ signal is reported on the bottom; the saturating L-glutamate concentration depolarises the illuminated area from the resting V_m (~-70 mV) to the reversal potential of AMPA receptors (0 mV). All calibrations were from single trials.
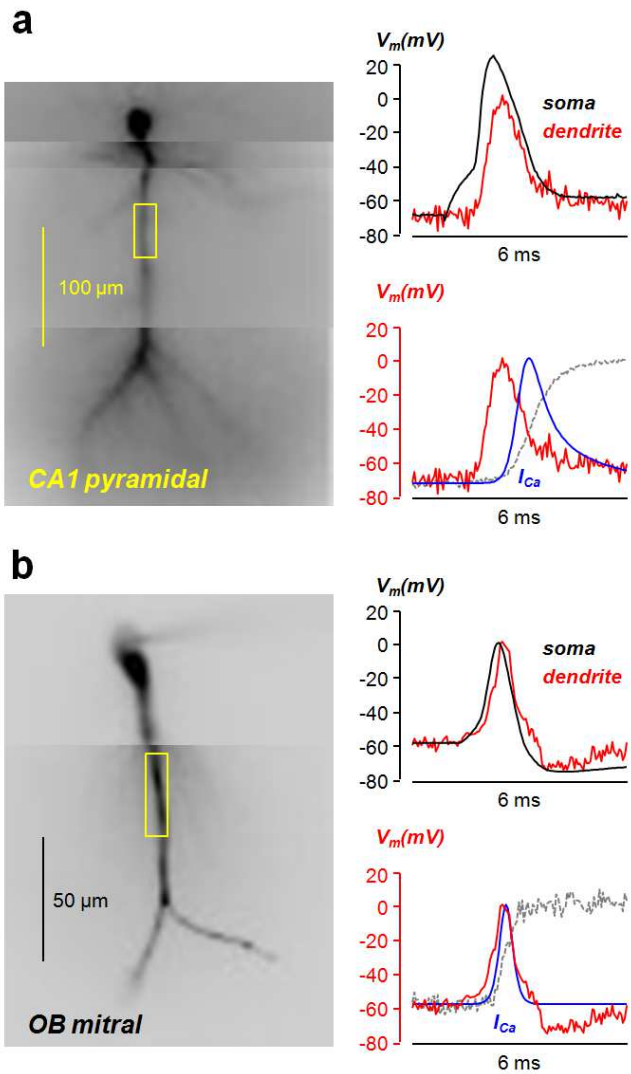
19

Fig. 5. Ca^{2+} currents associated with backpropagating action potentials in CA1 hippocampal pyramidal neurons and in olfactory bulb (OB) mitral cells (**a**) On the left, fluorescence image of CA1 hippocampal pyramidal neuron filled with JPW1114 and 2 mM OG5N with a region of the apical dendrite outlined. On the right, somatic V$_m$ change associated with an action potential (black trace) in the soma and in the dendritic region. The associated Ca^{2+} current kinetics, obtained with the fitting strategy from the raw Ca^{2+} signal (dashed gray trace), is shown in the bottom. (**b**) On the left, fluorescence image of OB cell filled with JPW1114 and 2 mM OG5N with a region of the principal dendrite outlined. On the right, somatic V$_m$ change associated with an action potential in the soma (black trace) and in the dendritic region (red trace). The associated Ca^{2+} current kinetics, obtained with the fitting strategy from the raw Ca^{2+} signal (dashed gray trace), is shown in the bottom (blue trace) superimposed to the dendritic action potential (red trace). Data, recorded at 20 kHz, were from averages of 4 trials. All experiments were performed at 32-34 °C.
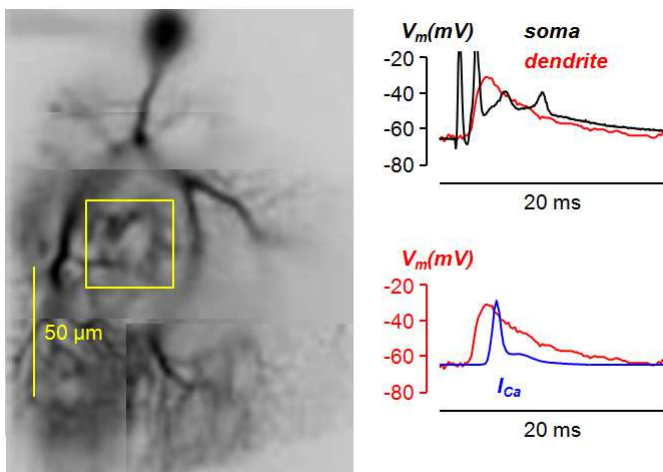
598

599

600

Fig. 6. Ca^{2+} currents associated with climbing fibre EPSPs in cerebellar Purkinje neurons. On the left, fluorescence image of PN filled with JPW1114 and 2 mM Fura-FF with a region of the dendrite outlined. On the right, somatic V$_m$ change associated with climbing fibre EPSP (black trace) in the soma and in the dendritic region. The associated Ca^{2+} current kinetics, obtained with the generalised method (24), is shown in the bottom. Data, recorded at 5 kHz, were from averages of 4
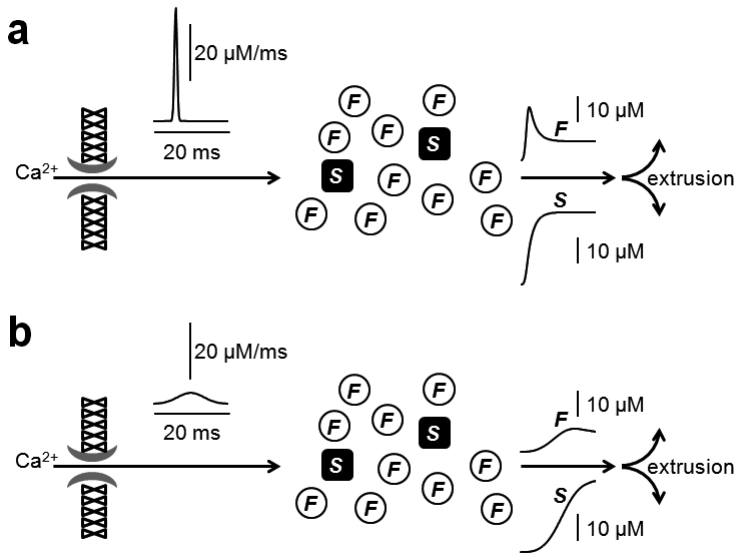
601

602

603

Fig. 7. Simulated activation of two different Ca^{2+}-binding proteins by Ca^{2+} currents. (**a**) In a cell containing 500 µM of a fast (*F*) buffer with K_{ON} = 5.7·10^8 M^{-1}s^{-1} and K_D = 10 µM, and 100 µM of a slow (*S*) buffer with K_{ON} = 4·10^8 M^{-1}s^{-1} and K_D = 0.4 µM, the curves on the right report the binding to Ca^{2+} of the *F* and *S* proteins following the fast Ca^{2+} current reported on the left. (**b**) Same as in the previous panel but following the fast Ca^{2+} current reported on the left.

604

605